Earth and Planetary Science Letters

Eustatic sea-level fall and global fluctuations in carbonate production during the Carnian Pluvial Episode

--Manuscript Draft--

Manuscript Number:	EPSL-D-21-01208R1
Article Type:	Letters
Keywords:	Eustasy; chronostratigraphy; Biostratigraphy, Sequence Stratigraphy; Late Triassic
Corresponding Author:	Marco Franceschi, Ph.D University of Trieste: Universita degli Studi di Trieste Padova, ITALY
First Author:	Xin Jin, PhD
Order of Authors:	Xin Jin, PhD
	Marco Franceschi, Ph.D
	Rossana Martini
	Zhiqiang Shi
	Piero Gianolla, PhD
	Manuel Rigo, PhD
	Corey J. Wall
	Mark D. Schmitz
	Gang Lu
	Yixing Du
	Xiangtong Huang
	Nereo Preto
Abstract:	In this paper, sea-level fluctuations during the Carnian Pluvial Episode (CPE) are investigated. A revision of published data from multiple successions worldwide indicates a sea-level drop that occurred in different geodynamic settings after the onset of the first of multiple carbon-isotope perturbations that characterize the CPE. New stable isotope data, zircon U-Pb geochronology, carbonate petrology, conodont and foraminifer biostratigraphy from the Carnian of the Sichuan Basin and comparison to the well-dated coeval successions of the Dolomites allow pinpointing with unprecedented precision this sea-level fall and determine that it occurred after the onset of the first, but prior to the third negative δ13C shift of the CPE. These lines of evidence indicate that such sea-level oscillation was eustatic. Facies analysis and sequence stratigraphy of units deposited during the ensuing sea-level rise in the Sichuan and Dolomites, further show that a Tethys-wide crisis of microbial carbonate production and drowning of carbonate platforms were followed by a recovery of marine calcification, widely testified by the deposition of oolitic bodies. Whereas a Tethys-wide recovery of microbial carbonate production is documented at the end of the Carnian, this increase in chemical calcification occurred earlier, at the beginning of the Tuvalian, and suggest that global transformations in carbonate systems coincident with the CPE were complex and share commonalities with other times in the geological record when a similar evolution was linked to ocean acidification.
Suggested Reviewers:	Yadong Sun yadong.sun@fau.de
	Spencer G. Lucas spencer.lucas@state.nm.us
	López-Gómez José jlopez@geo.ucm.es

	Ruffell Alastair a.ruffell@qub.ac.uk
	Paul B. Wignall P.B.Wignall@leeds.ac.uk

Trieste, June 5th 2022

Dear Professor Boswell Wing,

We thank you very much for allowing us to revise our manuscript (ID: EPSL-D-21-01208).

We provide a detailed response to all the comments of the Reviewers. Comments were very useful and we took them into high consideration, trying our best to revise our manuscript according to them.

In the revised version of the manuscript all changes are highlighted in red.

In the response file you will find:

The comments of reviewers set in Times New Roman normal font.

Our itemized replies are in Times New Roman bold font.

Modifications to the original manuscript are made according to the comments from the reviewers and some through self-improving.

The main point of concern expressed by one of the Reviewers, and echoed by the Associated Editor, was that the manuscript did not clearly show that the presented findings have global significance. In particular, the eustatic nature of the sea-level oscillation the paper focuses on was not thoroughly discussed.

In order to solve this important issue, we welcomed suggestion provided by the Associated Editor and attempted a review of the successions that worldwide display evidence of a sea-level fall compatible with the one observed in the Chinese section from which we retrieved new bio -chronostratigraphic, sedimentological and geochemical data presented in the paper.

In the revised manuscript, successions form Dolomites and Julian Alps (Italy), Northern Calcareous Alps (Austria), Central European Basin (Germany), Barents Sea, Aghdarband Basin (Iran), Iberia and Balearic Islands (Spain) are presented and correlated. In all these succession bio- magneto- chronostratigraphic constraints allow identifying a Julian sea-level oscillation that, being recorded in very different geodynamic settings can be reasonably considered eustatic.

This expanded discussion can be found in chapter 5.3 (line 296-415) of the revised manuscript.

We believe that now the global nature of one of the sea-level oscillations coincident with the CPE is better clarified and this, thanks to a detailed sequence stratigraphic correlation made possible by the new data from the Sichuan Basin, allows highlighting and putting into a wider context the commonality in facies evolution that eastern and western Tethys marine shallow water sedimentary systems developed during the transgressive phase following the eustatic fall.

All the figures were updated (with the exception of figure 2) accordingly.

We think that these modifications strengthen the paper and make it of potential interest for the wide readership of EPSL.

We truly appreciate your time and effort in considering our revised manuscript.

Yours sincerely,

Marco Franceschi on behalf of the co-Authors of this manuscript

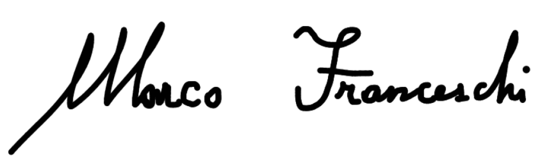

Here follow detailed responses to observations and comments of Reviewers. Replies are in bold.

Reviewer #1:

General Comments

Jin et al. did a nice works to explore the Eustatic sea-level fall and global fluctuations in carbonate production during the Carnian Pluvial Episode. In reading the manuscript sections on the radiometric dating, stable isotope geochemistry, carbonate petrology, and conodont and forminifer fossils, it seemed to me that these were original and substantive new contributions. The methods have been to be reasonably well explained and results clearly presented. I recommend it can be published after adding the comments I proposed below.

R: We carefully considered indications and comments provided by the Reviewers. Detailed responses are provided below.

Lines 50-51: "Several lines of evidence suggest that the CPE was a humid and Warm phase". What evidence (e.g., Clay, Plant or other something) suggests a humid and warm climate prevails? Please clarify. Perhaps some references need to be added (e.g., Roghi et al., 2010-3P; Rostási et al., 2011-3P; Mueller, 2016a, 2016b; Baranyi et al., 2019-GPC; Dal Corso et al., 2020-SA; Lu et al., 2021-PNAS; Peng et al., 2021-GS,London).

R: We modified the statement to include just the most relevant references (e.g., Baranyi et al., 2019; Dal Corso et al., 2020; Lu et al., 2021) while keeping the total number of references under 50, which is the maximum number permitted by the journal (line 62-63).

Line 64: Please provide references after "a major driver of differentiation process".

R: Hallam and Wignall (1999) was added (line 76-77).

Lines 67-68: Please provide references.

R: This statement were deleted in the revised MS.

Lines 82-83: Please provide references.

R: Metcalfe (2013) was added (line 97).

Lines 88-89: Here, I don't understand what is the basis for the division of Ma'antang Fm. into Carnian? Biostratigraphy or lithostratigraphy or chronostratigraphy? Please clarify and/or provide references.

R: This part was completely rewritten, and a new figure (Fig. 1C) was included to show the lithological composition, facies associations, and age of the Tianjinshan and Ma'antang formations. We have added a reference to Jin et al. (2019) where a comprehensive biostratigraphy clarifying the age of the Tianjinshan and Ma'antang formations can be found (line 95-107).

Line 198: Please change "800 mm" to "800 μm".

R: Corrected as indicated by the Reviewer (line196).

Lines 199-200: Please provide references.

R: Metcalfe (2013) was added (line197).

Lines 215-216: I think this sentence should be revised to "between the Late Anisian and the Late Carnian (243.7 ± 2.6Ma to 231.2 ± 3.6Ma)"

R: Corrected as indicated by the Reviewer (line214-215).

Line 242: What is the basis here for determining "hNCIE 3 coinciding with the boundary between Julian and Tuvalian"?

R: We rephrased the statement as "Subsequently, the hNCIE 3 occurs at 5 m above the hNCIE 2 with δ^{13}C values as low as 0.27‰ (Fig. 2). In contrast, no clear δ^{18}O excursion appears in the same level" (line241).

Line 242: What are the δ18O characteristics corresponding to hNCIE 3? Please describe it.

R: We added "In contrast, no clear δ^{18}O excursion appears in the same level" in the text

(line241).

Line 252: Please change "232-246Ma" to "246-232Ma".

R: This statement were deleted in the revised MS.

Line 257: All foraminifers in samples A to I whose distribution from Ladinian to Rhaetian? Please clarify and/or provide references.

R: We changed the statement, please see in the text (line257).

Line 287: exhibit a significant correlation ($R = 0.386$, $P<0.001$, $n = 105$; Fig. S4)? I don't think so. For me, $0.3<|R|<0.5$ is regarded as low correlation, $0.5<|R|<0.8$ is regarded as moderate correlation, $0.8<R<0.8$ is regarded as significant correlation.

R: We accept that the r value of 0.386 does indeed indicate a weak relationship. However, the correlation is significant because the p-value is telling us that an R value at least as high as 0.386 has only a <0.001 probability of being a result of chance. In other words, although the R value is low, it is significantly different from 0

Line 304-306: New references need to be added here (e.g., Li et al., 2021; Lu et al., 2021-PNAS). I note that two recent papers report high-resolution organic C-isotope record from terrestrial-marine transitional sediments of South China (Li et al., 2021) and terrestrial sediments of North China (Lu et al., 2021).

R: We rephrased this part, and Lu et al. (2021) and Li et al (2021) were added in the relevant place (line290).

Line 314: Reference error. Please change "Dal Corso et al., (2020)" to "Dal Corso et al., (2018)". In Fig. 5, the CPE composite of δ13C from Dal Corso et al., (2018-ESR; Line 518).

R: Thanks, Reviewer is right, but we deleted this reference in the revised version.

Line 547: Please change "Wignaall" to "Wignall".

R: Corrected as indicated by the Reviewer (line626).

Figure 1: where does the Fig. 1A come from? Please provide references.

R: Added the statement "modified from 1:50000 Geological Map of the Jiangyou Map Sheet published in regional geological survey report, 1996" (line558-559).

Figure 5: Here, I think the author should integrate SI Fig. 5 into Fig. 5, and then added the high-resolution organic C-isotope record from terrestrial-marine transitional sediments of South China as a correlation (Li et al., 2021).

R: In order to work within the constraints of figure numbers, we constructed carbon isotope correlations in Fig. S1, which includes typical terrestrial-marine CPE sections (Li et al., 2021 was included) and core.

Reviewer #2: Review EPSL for Jin et al., Eustatic sea-level fall and global fluctuations…

General: In general, some chapters are well-written, others are poor (Geological Setting, for example, but also many to follow). The whole study is based on one section which is not relevant for making the conclusions this study draws from this data set - and this data set is very limited. As is the paper is only good for a local journal but should definitely switch the focus. From a sedimentological standpoint this is over-interpreted, unfortunately. I cannot recommend acceptance or even major revisions at this point.

R: We have taken this general comment in serious consideration and revised the manuscript did our best in order to prove that our conclusions are not of local nature, but provide insights on a yet poorly considered aspect of the CPE time: eustatic sea-level oscillations.

In order to do so, we followed suggestion provided by the Associated Editor and provided a review of the successions that worldwide display evidence of sea-level fall at the CPE. In described successions, biostratigraphic constraints allow to correlate a sea-level fall that worldwide occurred in the Julian in different geodynamic settings. We believe that provided evidence is enough to consider this sea-level fall eustatic.

Abstract: OK as is and well written.

R: Thank you.

Introduction:

Line 51: Look it up but I think it is "Late Triassic" and not "late Triassic".

R: Corrected as indicated by the Reviewer (line62).

There is a paper by Rueffer and Zuehlke (1995?) in a book, Kluwer Academic Press that describes the sequence stratigraphy of the Dolomites. There is also another paper with the same topic by a French author that I currently do not remember. Jardin?

Sequence stratigraphy and sea-level changes in the Early to Middle Triassic of the Alps: a global comparison

B.U. Haq (Ed.), Sequence Stratigraphy and Depositional Response to Eustatic, Tectonic and Climatic Forcing, Kluwer, Amsterdam (1995), pp. 161-207

R: We appreciate Reviewer's suggestions. We checked the papers and in the majority of the studies, particularly Rueffer and Zuehlke (1995) who mainly concentrated on the Early to Middle Triassic, only a small part of the early late Triassic (Julian, early Carnian) is included. Our work concentrated on the entire Carnian (Julian and Tuvalian) focusing on the sea-level fall that thanks for the new data provide from the Chinese successions and to multiple evidence from a number of tectonically distinct basins can be reasonably considered eustatic.

Lines 77: Following: two distinct areas showing the same fluctuations do not necessarily prove that something is eustatic. It just shows that the same things happened in Sichuan and in the Dolomites. Could be both tectonics, and there is plenty of tectonics during sedimentation in the Dolomites (several papers by Doglioni, for example).

R: In order to argument on this important comment from the Reviewer we have consistently expanded discussion including successions from several localities worldwide: Dolomites and Julian Alps (Italy), Northern Calcareous Alps (Austria), Central European Basin (Germany), Barents Sea, Aghdarband Basin (Iran), Iberia and Balearic Islands (Spain), and South China

(this study), which are all tectonically independent basins. We think that provided evidence, together with the new data from the Chinese sections provided in the paper is enough to show that an eustatic sea-level oscillations occurred in the Julian during the CPE and exerted relevant influence in the evolution depositional systems during the Carnian Pluvial Episode.

Geological Setting:

There are several articles missing in the geological setting, and the writing is poor. Also, the geological setting just introduces the Chinese part of the succession and not the Dolomites.

R: The geological setting has been modified in the revised version. We highlighted "New data presented in this paper come from the Hanzeng section, located in the western Sichuan Basin (eastern Tethys, South China, Fig. 1A and B); other Carnian successions were also reviewed in this study, and they are located in the Dolomites and Julian Alps (western Tethys, Italy), in the Northern Calcareous Alps (western Tethys, Austria), in the Aghdarband Basin (Northeast Iran), in the Barents Sea (northern Pangea, Norway), in the Iberia and Balearic Islands (Spain), in the Central European Basin (northern peri-Tethyan realm). Their description can be found in the Discussion." (line 87-94).

Methods:

One section? Really? And then EPSL? This does not show anything.

R: See replies to comments above. It is true that geochemical, sedimentological and bio-chronostratigraphic data come from a section in the Sichuan basin, but they are put into a wider context through detailed correlation with the Western Tethys (where one of the better age-constrained record of the CPE exists) and to other coeval successions worldwide. Moreover, we have proposed a Tethys-wide sequence stratigraphic correlation that illuminates potentially relevant analogies in the evolution of sedimentary systems during eustatic oscillations coincident with the CPE. We believe that these findings may be of interest to a wide readership in the field of geoscience.

Results:

This needs to be a description. It is not, it is a mix of description and interpretation.

R: In the results section, an interpretation of the sedimentary environment and of the age that derives from fossil associations is somehow anticipated. This could be taken as a mix of description and interpretation - still, within each chapter, facies (fossils) are firstly reported, and conclusions on depositional environments and ages are only then drawn. In particular, the detailed description of facies in the supplementary materials keeps descriptions and environmental interpretations strictly separated. However, we still believe this was the best way to lay down the text. Alternatively, facies could be interpreted in a new specific chapter of the discussion, as well as conclusions on the age of the succession. While necessary to draw our conclusions, the depositional environment and age are not the main topic of our work. We found thus better not to incorporate these parts in the discussion, which we maintained focused on the main findings of our work.

Biostratigraphy

I can't judge this part

R:

Supplemental material:

Looking at the facie stable there is again a mix of description and interpretation in the "Microfacies description" part. There are also contradictions in the facies description by the way.

R: In the column "microfacies description" there is indeed one sentence with some interpretation which is (facies E.1): "Vertically oriented, cement-filled pores may represent the molds of cyanobacteral filaments." Now it was substituted by "Vertically oriented, cement-filled pores are present". We double-checked other parts and could not find contradictions in the facies descriptions, but without having an indication of where to look exactly, it is possible that we missed the point the Reviewer is making.

Highlights:

- New bio-, chrono-, chemostratigraphic and sedimentological data on the CPE
- Tethys wide correlation of carbonate platform successions across the CPE
- Correlations and sequence stratigraphy highlight an eustatic sea-level fall
- Results suggest global fluctuations in carbonate production during the CPE

Eustatic sea-level fall and global fluctuations in carbonate production during the Carnian Pluvial Episode

Xin Jin [1], Marco Franceschi * [2], Rossana Martini [3], Zhiqiang Shi [1], Piero Gianolla [4], Manuel Rigo [5, 6], Corey J. Wall [7], Mark D. Schmitz [7], Gang Lu [1], Yixing Du [1], Xiangtong Huang [8], Nereo Preto [5]

1. State Key Laboratory of Oil and Gas Reservoir Geology and Exploitation and Key Laboratory of Deep-time Geography and Environment Reconstruction and Applications of Ministry of Natural Resources, Chengdu University of Technology, Chengdu 610059, China

2. Department of Mathematics and Geosciences, University of Trieste, via Weiss, 2, 34128 Trieste, Italy

3. Department of Earth Sciences, University of Geneva, 13 Rue des Maraîchers, 1205 Geneva, Switzerland

4. Department of Physics and Earth Sciences, Università degli Studi di Ferrara, Via Saragat, 1, Ferrara 44100, Italy

5. Dipartimento di Geoscienze, Università degli Studi di Padova, Via G. Gradenigo 6, Padova, Italy

6. Istituto di Geoscienze e Georisorse–CNR, Via G. Gradenigo 6, Padova, Italy

7. Department of Geosciences, Boise State University, 1910 University Drive, Boise, ID 83725-1535, U.S.A.

8. State Key Laboratory of Marine Geology, Tongji University, Siping Road, Shanghai, 200092, China

*Corresponding author: mfranceschi@units.it

Abstract:

In this paper, sea-level fluctuations during the Carnian Pluvial Episode (CPE) are investigated. A revision of published data from multiple successions worldwide indicates a sea-level drop that occurred in different geodynamic settings after the onset of the first of multiple carbon-isotope perturbations that characterize the CPE. New stable isotope data, zircon U-Pb geochronology, carbonate petrology, conodont and foraminifer biostratigraphy from the Carnian of the Sichuan Basin and comparison to the well-dated coeval successions of the Dolomites allow pinpointing with unprecedented precision this sea-level fall and determine that it occurred after the onset of the first, but prior to the third negative $\delta^{13}C$ shift of the CPE. These lines of evidence indicate that such sea-level oscillation was eustatic. Facies analysis and sequence stratigraphy of units deposited during the ensuing sea-level rise in the Sichuan and Dolomites, further show that a Tethys-wide crisis of microbial carbonate production and drowning of carbonate platforms were followed by a recovery of marine calcification, widely testified by the deposition of oolitic bodies. Whereas a Tethys-wide recovery of microbial carbonate production is documented at the end of the Carnian, this increase in chemical calcification occurred earlier, at the beginning of the Tuvalian, and suggest that global transformations in carbonate systems coincident with the CPE were complex and share commonalities with other times in the geological record when a similar evolution was linked to ocean acidification.

1. Introduction

The Carnian Pluvial Episode (CPE) is a phase of prominent climate change occurred in the Late Triassic (e.g., Simms and Ruffell, 1989; Dal Corso et al., 2020). It was first recognized because a sharp lithological change characterized by the occurrence of terrigenous facies could be observed in several Carnian sedimentary successions worldwide (Simms and Ruffell, 1989). This lithological change was later shown to be associated with a major phase of perturbation in the global carbon cycle, characterized by multiple (at least four) negative shifts in the $\delta^{13}C$ of marine carbonates and terrestrial organic matter records (e.g., Dal Corso et al., 2018; Lu et al., 2021; Fig. S1), possibly at least in part due to the injection of large amounts of CO_2 into the atmosphere/ocean system during the emplacement of the Wrangellia Large Igneous Province (e.g., Furin et al., 2006; Dal Corso et al., 2020; Lu et al., 2021; Mazaheri-Jorari et al., 2021). Hg enrichment and an increased input of non-radiogenic Os in coeval sedimentary deposits support the LIP volcanism hypothesis (Tomimatsu et al., 2021; Lu et al., 2021; Mazaheri-Jorari et al., 2021; Fig. S1). Evidence from clay minerals and palynofloras suggests that the CPE was a humid and warm phase that stands out in the Late Triassic climate (e.g., Baranyi et al., 2019; Dal Corso et al., 2020; Lu et al., 2021), and may have even been characterized by hyperthermal intervals and times of extremely intense rainfall (Rigo et al., 2012; Trotter et al., 2015; Sun et al., 2016). The coincidence of the CPE with a major faunal and floral turnover (e.g., Dal Corso et al., 2020) and with important large-scale changes in shallow water carbonate environments (Hornung et al., 2007; Stefani et al., 2010; Gattolin et al., 2015; Jin et al., 2020) indicates that the CPE had a profound and multifold impact on the Carnian marine and continental environments with consequences that carried their effects in the ages to come (Dal Corso et al., 2020).

Whereas much work has been done in assessing the global expression of the CPE isotope perturbation in the geological record, and evaluating the associated changes in marine and continental environments (e.g., Trotter et al., 2015; Sun et al., 2016; Dal Corso et al., 2018; Baranyi et al., 2019; Shi et al., 2019), less attention has been so far dedicated to sea-level changes. Sea-level variations, however, are a major driver of sedimentation processes and exert a huge impact on ecosystems (Hallam and Wignall, 1999).

In this paper, we combine a critical assessment of literature data concerning sea-level variations in the Carnian with new data on biostratigraphy, high precision U-Pb zircon dating, carbon-isotopes and sedimentology from a Carnian shallow water carbonate succession of the Sichuan Basin (South China), to analyze sea-level oscillations coincident with the CPE. Results highlight Tethys-wide eustatic sea-level changes strictly associated with the CPE, and reveal commonalities in facies evolution of carbonate systems that shed further light on the large-scale oceanographic changes associated to the Carnian Pluvial Episode.

2. Geological setting

New data presented in this paper come from the Hanzeng section, located in the western Sichuan Basin (eastern Tethys, South China, Fig. 1A and B); other Carnian successions were also reviewed in this study, and they are located in the Dolomites and Julian Alps (western Tethys, Italy), in the Northern Calcareous Alps (western Tethys, Austria), in the Aghdarband Basin (Northeast Iran), in the Barents Sea (northern Pangea, Norway), in the Iberia and Balearic Islands (Spain), in the Central European Basin (northern peri-Tethyan realm). Their description can be found in the Discussion.

The Western Sichuan Basin is located at the northwestern margin of the South China Block (Fig. 1A), and was a part of Eastern Tethys during the Late Triassic (e.g., Metcalfe, 2013). The basin transitioned from a marine cratonic basin in the Proterozoic-Middle Triassic period into a foreland basin in the Late Triassic-Late Cretaceous (e.g., Li et al., 2014). A flexural forebulge unconformity between the Tianjinshan Fm. (uppermost Leikoupo Fm., Middle Triassic) and Ma'antang Fm. (Upper Triassic) marks the base of the foreland basin mega-sequence (e.g., Li et al., 2014). Shi et al. (2019) and Jin et al. (2019) propose to consider the forebulge unconformity to be in the uppermost part of the Tianjinshan Fm. This because laminated microbialites partly dolomitized of Carnian age (Jin et al., 2019; Fig. 1C), a lithology that is characteristic of the Tianjinshan Fm., continue above the unconformity and the passage at the Ma'antang Fm. is marked by the occurrence of bioclastic and oolitic limestones later followed by silty mudstones and siltstone (Fig. 1C). The Ma'antang Fm. is referred to a transgressive carbonate ramp in its lower part, while its upper portion is characterized by terrigenous-rich units (Wu, 1989; Li et al., 2014; Jin et al., 2019; Fig. 1C).

3. Methods

A total of 69 bulk rock samples from Hanzeng section were prepared as thin sections which were further investigated under a polarizing optical microscope at the Institute of Sedimentary Geology of the Chengdu University of Technology. Eight rock samples were collected for conodont biostratigraphy. Sample preparations followed Jin et al. (2019). Sixteen samples (labeled A to Q in Fig. 2) were collected from the base up to ca. 50 m of the Hanzeng section for foraminifer biostratigraphy. From a bentonite layer identified right above Karst 1 zircon crystals were extracted for radiometric (U-Pb) dating (Fig. 2). LA-ICP-MS was used on 83 grains at the State Key Laboratory of Marine Geology, Tongji University, China, for a preliminary age screening of the zircon population in the bentonite. The obtained age data are reported at 1σ level of uncertainty, whereas uncertainties for the weighted mean ages are given with a 95 % confidence level (2σ). Eight grains were selected for isotope dilution thermal ionization mass spectrometry (CA-ID-TIMS) following Schmitz and Davydov (2012), which was done at Department of Geosciences, Boise State University. One hundred and five bulk rock samples were collected from the Hanzeng section for $\delta^{13}C$ and $\delta^{18}O$ analyses. A total of 66 of which were tested by a Delta V Advantage Isotopic Ratio Mass Spectrometer linked to a Gasbench II device at the Department of Geosciences of the University of Padova. A total of 39 of which were analyzed in a GasBench II coupled in continuous flow through Thermo Finnigan MAT 253 Mass Spectrometer at College of Earth Sciences, Chengdu University of Technology. All analyses are further described in the Supplemental Information (SI), and data are listed in the Supplemental Dataset (SD).

4. Results

4.1. Sedimentology of the Hanzeng section

The Hanzeng section, focus of this study, is located near Hanzeng town (31°47' N; 104°37' E; Fig. 1B) and encompasses the uppermost Tianjingshan Fm. and most of the Ma'antang Fm. (Fig. 2). Two paleokarst surfaces (Karst 1 and Karst 2) in Fig. 2 and Fig. S2A have been highlighted at Hanzeng, and are marked in the field by irregular surfaces with evidence of karst dissolution (Fig. S2B and C). The lowermost surface (Karst 1 at the ~11.3 m) is within the uppermost Tianjingshan Fm. The boundary between Tianjingshan and the Ma'antang formations at Hanzeng section is placed at Karst 2 (~25 m).

In the Hanzeng section, 17 microfacies associations were identified (A1 to A3; B1 and B2; C1 to C3; D1 to D4; E1 to E3; F1 and F2; Fig. 2). The detailed descriptions of the microfacies associations can be found in the SD. In this study, the lower 25 meters successions make up the topmost Tianjingshan Fm. (Fig. 2). The uppermost Tianjingshan Fm. succession is made of peritidal cycles referable to the inner portion of a microbial carbonate platform (See details in the SI). The overlying Ma'antang Fm. can be interpreted as a peritidal inner platform from ~25 meter to 26.5 m (Fig. S3) and as a ramp from ~26.5 m to the top (Fig. 2). The overlying darker part with cherty nodules (~32.5 m to 64.5 m; Fig. S2A and E) of the Ma'antang Fm. deposited in deeper portions of the carbonate ramp (also see facies model in Fig. S3).

The outer ramp is dominated by overall fine-grained sediments with reworked skeletal grains and spiculae of siliceous sponges. Carbonate mud is ubiquitous, none of the grains is from phototrophic organisms. In the middle ramp (~64.5 m to 106 m), a sponge-microbial reef occurs below the wave base, which must have been within the photic zone, since a few phototrophic organisms are found (e.g., *Cayeuxia*). At the top of the Hanzeng section, well-sorted grainstones with ooids and worn skeletal grains can be interpreted as carbonate sand shoals, nearby a reef which reworked elements are sometimes found floating in the grainstones. This facies association deposited in an inner ramp setting (Fig. 2). A more detailed facies description of the Hanzeng section is also provided as SI.

4.2. Biostratigraphy

4.2.1. Conodonts

All the eight processed samples collected for conodont biostratigraphy yielded conodont elements with a Color Alteration Index (CAI) of 1. The most biostratigraphically significant were obtained in the first few meters of the Ma'antang Fm. (meters 26.5-30 in Fig. 2): *Paragondolella polygnathiformis*, *Paragondolella* aff. *P. foliata* (Fig. S4-1) and *Paragondolella praelindae.* The latter two have been reported from the uppermost Julian in Italy (Rigo et al., 2007). *Paragondolella praelindae* is the index species of the Julian *P. praelindae* Zone, described in Rigo et al. (2018), which includes the onset of the CPE (e.g., Rigo et al., 2007, 2018; Dal Corso et al., 2018). *Paragondolella* aff. *P. foliata* was so far documented only in the uppermost Julian (lower Carnian), always associated to other typical Julian conodonts, such as *P. tadpole, P. inclinata, P. praelindae* and *Gladigondolella* sp. (Rigo et al., 2007, 2018). Slightly above, the conodont *Hayashiella tuvalica* (Fig. S4-2, 3) was recognized along with *Paragondolella noah*, *P. maantangensis* (Fig. S4-5) and *P. oertlii* (Fig. S4-4). This conodont assemblage corresponds to the conodont *H. tuvalica* Zone of Rigo et al. (2018), the lowermost Tuvalian conodont Zone.

4.2.1. Foraminifers

Benthic foraminifers have been found in 16 samples (A to Q) from ~4 m from the bottom of the Hanzeng section up to ~51.5 m (Fig. 2). The originally aragonitic species appear strongly recrystallized (i.e., Fig. S5: 1, 7-9, 15-18, 21, 24) with a micritic rim, as often observed in the Triassic successions. Conversely, the preservation of the other types of walls (i.e., porcelaneous, microgranular and hyaline) is rather good. The foraminiferal assemblage is relatively homogenous along the sampled interval, although not all forms are found in a single sample. It includes originally aragonitic *Aulotortus* ex. gr. *A. sinuosus*, *Aulotortus impressus*, *Triadodiscus eomesozoicus*, the glomospiroid Involutinina *Parvalamella friedli* and the duostominiid *Variostoma pralongense*. *T. eomesozoicus*, although completely recrystallized, is easily recognizable by its morphology and size of the test, as well by its association with other foraminifers. Concerning *Parvalamella friedli*, Rigaud et al. (2012) emphasize its large morphological variability and that the specimens described from the Black Marble Quarry (Oregon, Wallowa terrane, U.S.A.) are proportionally smaller than Tethyan forms, which may reach 800 µm in diameter, and exceptionally more. Our specimens are very large (Fig. S5: 15-18), which is consistent with the position, in the Eastern portion of Tethys, of the South China block during the Late Triassic (Metcalfe, 2013).

The microgranular and agglutinated foraminifers are relatively well diversified, with *Gaudryina triadica*, "*Trochammina*" *alpina*, *Endotriada tyrrhenica* and "*Valvulina*" *azzouzi*. Porcelaneous *Gsolbergella spiroloculiformis* and *Agathammina iranica* also occur, together with representatives of the family Nodosariidae.

The foraminiferal association is characteristic of shallow water, lagoonal and/or inner ramp environment of Tethys and Panthalassa (Chablais et al., 2011 and references therein).

4.3. LA-ICP-MS zircon U/Pb ages

As evident from cathodoluminescence (CL) (Fig. S6A), the volcanic zircon grains from the sample Hanzeng are mainly prismatic fragments or euhedral crystals. The large majority of the zircons show well-developed oscillatory zoning. Most zircons range in length from ~50 µm to ~150 µm with length/width ratios of ~2:1 to 3:1 (Fig. S6A). The internal features indicate a magmatic origin (Rubatto and Gebauer, 2000). The age distribution of volcanic zircons of sample Hanzeng shows a large dominance $^{206}Pb/^{238}U$ age group (n=53) between the Late Anisian and Late Carnian (243.7 ± 2.6 Ma to 231.2 ± 3.6 Ma), which is centered at 237.02 ± 0.97 Ma (Fig. S6B and C). The analytical results are listed in SD.

4.4. TIMS zircon U/Pb ages

CL-imaging of zircon crystals revealed a consistent population of moderately to brightly luminescent, oscillatory zoned crystals. A small number of crystals have irregularly shaped, relatively non-luminescent cores overgrown by the aforementioned luminescent, oscillatory rims. Eight grains were selected for CA-TIMS analysis on the basis of the uniform CL pattern, consistent in-situ U-Pb dates and avoiding those crystals with resorbed non-luminescent cores. All eight analyses are concordant and equivalent, with a weighted mean $^{206}Pb/^{238}U$ date of 238.430 ± 0.047(0.13) [0.28] Ma (MSWD = 0.51) (Fig. S6D and E), which is interpreted as dating the eruption and deposition of this ash bed.

4.5. $\delta^{13}C$ and $\delta^{18}O$

The carbonate carbon and oxygen isotopic data of the Hanzeng section are shown in Figure 2. $\delta^{13}C$ values range from –2.6‰ to +3.4‰, and have an average $\delta^{13}C$ value of +1.7‰. $\delta^{18}O$ values range from –8.5‰ to –1.3‰, and the mean value is –3.9‰. These values fall in part within the range of the isotopic composition of Carnian articulate brachiopods (Fig. S7 in the Supplemental Information; see Korte et al., 2005). Three negative carbon isotopic excursions can be identified (hNCIEs in Fig. 2), which overlap on a longer oscillatory trend from higher, to lower, and then again to higher $\delta^{13}C$ values. The first carbon isotopic excursion (hNCIE 1) is found below the Karst 1 surface (Fig. 2), where the values of both the $\delta^{13}C$ and $\delta^{18}O$ are depleted in heavy isotopes with respect to the rest of the section. The second negative shift (hNCIE 2) has an amplitude of ca. 4.7 ‰ in $\delta^{13}C$, in correspondence with the Karst 2 unconformity, and is paired with a similar negative excursion of the $\delta^{18}O$ (Fig. 2). Subsequently, the hNCIE 3 occurs at 5 m above the hNCIE 2 with $\delta^{13}C$ values as low as 0.3‰ (Fig. 2). In contrast, no clear $\delta^{18}O$ excursion appears in the same level. This negative shift is then followed by a long recovery phase up to 65 m in the Hanzeng section. The top of the section is characterized by an upright trend of the $\delta^{13}C$ values (Fig. 2).

5. Discussion

5.1. Bio-chronostratigraphy of Hanzeng section

Radiometric dating of the zircons collected from the tuff layer above Karst 1 surface yields 238.430 ± 0.047 Ma, indicating a late Ladinian age. Such age is consistent with those yielded by the volcanic zircons commonly observed in the Upper Triassic units of Sichuan Basin which testify for magmatic activity during the Indosinian orogenic collision at the west margin of Yangzi plate (e.g., Yan et al., 2019). Subsidence, and consequent sedimentation, in the Western Sichuan foreland Basin began in the Late Triassic (e.g., Li et al., 2014), therefore suggesting that Karst 1 could be due to Ladinian peripheral bulging connected to the Indosinian Orogeny.

Between Karst 1 and Karst 2, Ladinian to Carnian deposits are found. Samples A to I (Fig. 2) yielded foraminifers whose distribution ranges from Ladinian to Rhaetian, such as the foraminifer *Gsolbergella*, which distribution ranges from Carnian to Rhaetian (Rettori et al., 1998) has been found in sample J (Fig. 2). Thus, biostratigraphy allows assigning beds between Karst 1 and Karst 2 at Hanzeng a Ladinian age up the FAD of *Gsolbergella* and a Carnian to Rhaetian age from this FAD on. The Carnian age of the upper part of the Tianjingshan Fm. has been also indicated by Jin et al. (2019).

Above Karst 2, biostratigraphically significant conodont assemblages are found and consist of typical Carnian pectiniform elements such as *Paragondolella polygnathiformis*, *Paragondolella* aff. *P. foliata*, *P. praelindae*, *Hayashiella tuvalica*, *Paragondolella noah*, *P. maantangensis* and *P. oertlii*. *Paragondolella polygnathiformis* is a long-ranging species present until the middle Tuvalian and it was found along with *Paragondolella* aff. *P. foliata* and *P. praelindae* from meter level 26.5 to meter level 28 in the section. The two latter species are reported to occur together in the uppermost Julian (Rigo et al., 2007). The conodont *Hayashiella tuvalica* was recognized about 1.5 m (meter level 29.5) above the occurrence of *Paragondolella* aff. *P. foliata*, and occurs together with *Paragondolella noah*, *P. maantangensis* and *P. oertlii*. This conodont assemblage corresponds to the conodont *H. tuvalica* Zone of Rigo et al. (2018), which is the lowermost Tuvalian conodont Zone. Thus, we place the Julian-Tuvalian boundary between meters 28 and 29.5 of the Hanzeng section on the base of the first occurrence of *H. tuvalica*. These findings indicate that rocks between the FAD of foraminifer *Gsolbergella* and Karst 2 are Carnian and more specifically Julian, as the Julian/Tuvalian transition has been identified above, in the Ma'antang Fm. In sum, biostratigraphic and radiometric data from Hanzeng section make it possible bracketing Karst 2 to the Julian time (Fig. 2).

5.2. The Carnian Pluvial Event at Hanzeng

As discussed above, hNCIE 1 and 2 at Hanzeng likely products of meteoric diagenesis because associated to very negative $\delta^{18}O$, whereas the hNCIE 3 at the Julian/Tuvalian boundary can be considered as reflecting the original carbon isotopic compositions of Carnian sea water (See also SI).

As mentioned in the Introduction, detailed bio- and chemostratigraphic studies have shown that the CPE, which onsets at the Julian 1/Julian 2 transition, encompasses a large portion of the Tuvalian and is a multi-phase event characterized by at least four NCIEs (e.g., Sun et al., 2016; Dal Corso et al., 2018; Baranyi et al., 2019; Li et al., 2021; Lu et al., 2021; Fig. S1). The third NCIE of the CPE has been dated through ammonoid biostratigraphy between the latest Julian and the earliest Tuvalian (Dal Corso et al., 2018; Fig. S1). The radiometric and biostratigraphic data presented in this work show that hNCIE3 at Hanzeng section culminates at the Julian/Tuvalian transition and therefore we correlate this negative isotope shift with the third NCIE of the multi-phase CPE $\delta^{13}C$ perturbation (Fig. 2 and Fig. S1).

5.3. An eustatic sea-level fall coincident with the CPE

Data from Hanzeng section highlight the presence of a Julian sea-level fall, testified by a subaerial unconformity (Karst 2), which predates the third NCIE of the CPE (Fig. 2). As there is no evidence for strong condensation in the carbonate facies, the sea-level fall corresponding to Karst 2 most likely caused a significant hiatus that obliterates the majority of the Julian at Hanzeng. This is also confirmed by the partial record of the CPE $\delta^{13}C$ perturbations, of which only the third NCIE above Karst 2 is recorded at Hanzeng (Fig. 3 and Fig. S1).

Several successions worldwide display evidence of sea-level oscillations around the CPE. According to Haq's (2018 and references therein) reappraisal of Triassic sea-level fluctuations, a major sea-level fall in the Carnian occurred at 233.5 Ma (TCa2 of Haq, 2018), close to the onset of the CPE that has been dated to the boundary between Julian 1 and Julian 2 (*Trachyceras aoonoides-Trachyceras austriacum* ammonoid Zone boundary).

Such seal-level fall has been constrained through magnetostratigraphy, ammonoid, conodont and/or pollen biostratigraphy in the following areas (Fig. 3).

Dolomites and Julian Alps (Italy).

In this area, the Carnian succession consists of the Cassian Dolomite and its basinal correlative San Cassiano Fm., both followed by the Heiligkeuz and Travenanzes formations (Fig. 3). The Cassian Dolomite is made of shallow water microbial carbonates, the San Cassiano Fm. is mainly composed of calcareous turbidites and marls; the Heiligkeuz Fm. is mainly composed of coarse silicislastics with interbedded skeletal and oolitic limestones; the Travenanzes Fm. consists of clays and dolomites referred to a dryland river system to marginal marine coastal system (Stefani et al., 2010; Breda and Preto, 2011). In the Julian Alps, located east of the Dolomites in the Italian Southern Alps, the Carnian shallow water succession starts with, the Schlern Dolomite, equivalent of the Cassian Dolomite in the Dolomites, followed by the Conzen Fm., the Tor Fm. and the Portella Dolomite. This latter correlates to the oolitic top of the Heiligkreuz Fm. (Gianolla et al., 2003) (Fig. 3). The Carnian succession ends with the Carnitza Fm., dominated by nodular, cherty lime-mudstones (Gianolla et al., 2003).

A sea-level fall that in the basinal succession (San Cassiano Fm.) can be dated to the Julian 1-Julian 2 thanks to ammonoid, conodonts and pollens is responsible of a subaerial unconformity between the Cassian Dolomite and the Heiligkreuz Fm. and between the correlative "Schlern" and the Conzen formations (Fig. 3, Gianolla et al., 1998; Stefani et al., 2010; Dal Corso et al., 2018). In the sequence stratigraphic scheme proposed by Gianolla et al. (1998) this sea-level fall is the base sequence boundary of the Car 2 depositional sequence (Fig. 4).

Northern Calcareous Alps (Austria).

The Lower Carnian succession in the Northern Calcareous Alps (NCA; Fig. 3) is characterized by the presence of a depositional system dominated by large flat-topped carbonate platforms (Wetterstein Fm.) interfingering with a basinal succession made by nodular limestones and shales (Reifling Fm.) (Fig. 3; Lein et al., 2012). The overlying Göstling Mb. and Reingraben Shales (Hornug et al., 2007; Mueller et al., 2016), are composed respectively by reworked neritic calciturbidites and black shales, which are overlain by silt- and sandstones of the Lunz Fm. (late Julian 2 to Tuvalian 2), followed by the carbonate marginal marine Opponitz (Tuvalian 3, Hornung et al., 2007; Lein et al., 2012; Mueller et al., 2016). In the NCA the record a sea-level fall is locally documented by a marked, karstified subaerial unconformity on top of the Wetterstein Fm. (Lein et al., 2012) while, in basinal areas, the onset of sea-level fall is recorded by the reworked calciturbidites of the Göstling Mb., followed by the terrigenous input of the Lunz Fm.. This sequence boundary can be dated to the uppermost Julian through ammonoid-, pollen- and conodont biostratigraphy (e.g., Hornung et al., 2007; Muller et al., 2016).

Central European Basin (Germany).

The Late Triassic Central European Basin (CEB; Fig. 3) was characterized by a shallow marine epicontinental sea of the northwestern peri-Tethyan realm (e.g., Zhang et al., 2020). The Carnian successions in the northern CEB begins with the shaly-evaporitic Grabfeld Fm. (Fig. 3), which is overlain by the predominantly fluvio-deltaic Stuttgart Fm. (e.g., Zhang et al., 2020). The Weser Fm. (Upper Gipskeuper) is at the top, and it is made of playa- to sabkha-like deposits (e.g., Zhang et al., 2020). The base of the Stuttgart Fm., at the basin' margins, record an important unconformity (named *Diskordanz* D2, cf. Kozur and Bachmann, 2010), sometimes deeply incised on the underlying formations (e.g., Zhang et al., 2020). This unconformity is dated to uppermost Julian thanks to biostratigraphy and magnetostratigraphy (Kozur and Bachmann, 2010; Zhang et al., 2020).

Barents Sea.

The Barents Sea was located at higher latitudes (30° N to 60° N) during the Triassic (Fig. 3), and the Carnian is represented by the Kapp-Toscana Group that comprises fluvial and deltaic deposits (Klausen et al., 2020). Deltaic deposits span the Ladinian to early Norian period and are assigned to the Snadd Formation (Klausen et al., 2020).

Within the Snadd Fm. an important sea-level fall occurs and is followed by the progradation of the largest delta system documented so far in Earth history (Klausen et al., 2020; Fig. 3). This sea-level fall has been dated to approximately the Julian/Tuvalian boundary thanks to the palynological investigations (Vigran et al., 2014).

Aghdarband Basin (Iran).

The Aghdarband Basin (Northeast Iran; Fig. 3) was located at 35-45° N latitude and adjacent to a volcanic arc during the Late Triassic (Mazaheri-Johari et al., 2022). Palynostratigraphy allows dating the uppermost Sina Formation (predominantly tuffaceous sandstones) and the lower to middle portion of the Miankuhi Formation (polygenic conglomerate beds with interbedded sandstones, shales and coal seams) to the Carnian (Mazaheri-Johari et al., 2022). According to Mazaheri-Johari et al. (2022) the two units are separated by an unconformity that is dated to the Julian by palynostratigraphy (Mazaheri-Johari et al., 2021).

Iberia and Balearic Islands (Spain).

In Iberia and Balearic Islands, the Carnian succession is included in the Valencia Keuper Group and comprises the evaporitic Jarafuel Formation, the sandstones of the Manuel Formation and the claystones of the Cofrentes Formation (Fig. 3). The boundary between the Jarafuel and Manuel formations is an unconformity related to a sea-level fall that can be ascribed to the early Carnian through palynostratigraphy (Ortì et al., 2017). Notably, in this area there is evidence of incises valley systems cutting through the Paleozoic basement, and therefore a sea-level fall of several tens of meters can be estimated (Barenechea et al., 2018).

In the light of new data from the Sichuan Basin, and the review of literature presented above, it appears that a significant sea-level fall that that occurred during the CPE time is documented worldwide in several Carnian successions (Fig. 3) and that the sedimentary record of the intervening transgression started before the time of the third CPE NCIE. Since such correlative sea-level fall is recorded in different geodynamic contexts, ranging from the western to the eastern Tethys in longitude and from the Boreal realm to the tropics in latitude, it is fair to conclude that it is part of a Julian eustatic sea-level oscillation occurred within the CPE and terminated before the Julian–Tuvalian transition.

One side implication of the correlation of Karst 2 in Hanwang with the eustatic Julian sea-level fall is that this reinforces Shi et al. (2019) and Jin et al. (2019) interpretation of Karst 1 as the expression of the forebulge unconformity at the base of the Carnian sequence of the Sichuan Basin.

The identification of the Julian eustatic sea-level drop opens questions about its possible causes. Current evidence indicates that the Carnian was a continental ice-free time and therefore glacio-eustasy appears unlikely as a driving mechanism. On continents (e.g., IVU Basin in South America and Jiyuan Basin in North China), coeval large lake systems existed in the Carnian (Lu et al., 2021; Benavente et al., 2022). Franceschi et al. (2019) has suggested that limno-eustatic phenomena could have been at play during the CPE. The identification of the eustatic nature of the Julian sea-level fall, and its coincidence with a phase of expansion of lacustrine systems on continents, may further support this hypothesis. Its testing, however, requires a detailed correlation between the marine and the continental realm that could prove that increased water storage in lacustrine systems actually coincided with the sea-level fall.

5.4. Facies evolution at Hanzeng as compared to the Western Tethys: evidence of a Tethys-wide carbonate production crisis and recovery during the CPE

We propose a sequence stratigraphic correlation and comparison of facies evolution between the Sichuan Basin (Hanzeng section) and the Western Dolomites, to recognize an eustatic Julian sea-level fall associated with the onset of the CPE, occurring between the first and the third NCIE of the multiphase isotope perturbation. This correlation is possible because of the established high-resolution bio-, chemo- and sequence stratigraphic framework of both the Sichuan Basin and the Western Dolomites and since there two basins were located at the extremities of the Tethys Ocean (Fig. 4). For the sequence stratigraphic correlation, we use the framework proposed by Gianolla et al. (1998) according to which the Julian sea-level fall is the sequence boundary between the Car 1 and Car 2 depositional sequences. The paleogeography in the Dolomites was characterized by several high relief carbonate platforms (Cassian Dolomite) adjacent to deeper basins (Stefani et al., 2010). The CAR 2 sequence in the Western Dolomites is mostly represented by the Heiligkreuz Fm. (Fig. 4), a mixed carbonate/terrigenous unit deposited during the CPE which filled up the periplatform basins and leveled the former submarine paleo-topography (Preto and Hinnov, 2003; Stefani et al., 2010; Gattolin et al., 2015).

The stratigraphy of the CAR 2 sequence in the Western Dolomites is displayed in Figure 4 in the sections of Torri del Falzarego and Dibona Hut (Preto and Hinnov, 2003), which represent platform and basin environments, respectively. The CAR 2 lower sequence boundary, related to the Julian eustatic sea-level fall, is represented by a karst surface on the top of lower Julian carbonate platforms (Cassian Dolomite at Torri del Falzarego in Fig. 4). The correlative conformity in the adjacent basins (Dibona section) is marked by the deposition of proximal turbidites and mass-flow coarse deposits (coarse sand and conglomerate) on top of offshore muds (Fig. 4). In deeper water settings, record of the falling phase of the Julian eustatic oscillation can be found and the Falling Stage System Tract (FSST) and Lowstand System Tract (LST) of CAR 2 sequence are preserved (Gattolin et al., 2015). The FSST is represented by a succession of coarse siliciclastic deposits and grainstone beds alternated to offshore muds, and includes microbial patch reefs with calcareous sponges and other metazoans, often without photosynthesizing biota. At Dibona, the FSST terminates with a downstepping set of clinoforms made of dolomitized grainstone, which is onlapped by mixed carbonate-siliciclastic peritidal cycles of the top LST. Above, the Transgressive System Tract (TST) is made of a mixed carbonate-clastic succession which terminates with few meters of nodular lime mudstones, locally bearing ammonoids and conodonts belonging to the uppermost Julian–lowermost Tuvalian, with marly interlayers and rare chert nodules (Preto and Hinnov, 2003). These nodular limestones mark the Maximum flooding zone (Mfz) of the CAR 2 depositional sequence in the Dolomites. The Mfz and High Stand System Tract

(HST) of CAR 2 sequence are preserved both above former carbonate platforms and above former basins. The HST is made of meter-scale beds to >10 m banks of dolomitized oolitic grainstones and/or hybrid arenites, with cross bedding (Fig. 4). This lithological unit has a thickness of few tens of meters, but displays a considerable lateral continuity as it can be found in contiguous basins at a distance of hundreds of kilometers. Above this oolitic body, the boundary of the following CAR 3 depositional sequence is another subaerial unconformity (e.g., Breda and Preto, 2011; Fig. 4).

At Hanzeng, the Karst 2 surface, interpreted as the local expression of the Julian eustatic sea-level fall, is found on top of stromatolitic carbonates of the Julian Tianjinshan Fm., which are indicative of a peritidal carbonate platform environment (Fig. 2). The CAR 2 sequence develops in the following Ma'antang Fm. Since at Hanzeng this latter deposited on top of a former carbonate platform, and likely because of low subsidence rates deposits that could be referred to the FSST, LST and most of the TST are missing at Hanzeng section (Fig. 4). Bioclastic and cherty limestones, referable to an outer ramp to deep basin environment in the lower portion of the Ma'antang Fm. (Fig. 2 and Fig. S2E), represent the uppermost TST and the Mfz, which is followed, with a shallowing-upward trend, by bioclastic and oolitic limestone referable to the HST (Fig. 2 and 4). The top of CAR 2 sequence at Hanzeng section is unfortunately missing because of tectonics, nevertheless, Wu (1989) indicated that the bioclastic oolitic unit was overlain by a terrigenous succession (Huanglianqiao section in Fig. 1B and Fig. 4). Although a precise biostratigraphic framework is missing for Huanglianqiao, the evolution observed there closely resembles that seen in the Western Dolomites where the marginal marine Travenanzes Fm. follows the mixed carbonate-siliciclastic Heiligkreuz Fm. (Fig. 4). The base of the terrigenous succession at Huanglianqiao may therefore represent the CAR 3 sequence boundary in the Sichuan Basin (Fig. 4).

Facies evolution in the Hanzeng area (Eastern Tethys) and Western Dolomites (Western Tethys) shows a deepening-upward trend after the Julian sea-level fall (the TST of CAR 2: Fig. 4). Such evolution indicates that carbonate production was for a certain time unable to match the rate of creation of accommodation during the transgressive part of the eustatic oscillation and shallow water environments deepened (Fig. 5).

The following, regressive part of the CAR 2 depositional sequence, testifies for a recovery of carbonate production that was able to outpace the rate of accommodation creation. Roughly at the same time, both in Hanzeng area and in the Western Dolomites, the CAR 2 HST contains thick oolitic bodies (Fig. 4 and 5). This may simply reflect a coincident analogous evolution of the sedimentary environment; nevertheless, it has been shown that the deposition of oolitic bodies can be associated with crises of carbonate production coincident with carbon isotope perturbations (Fig. 4 and 5). Notable examples have been described in other times of the geologic record, e.g., in the Early Triassic and Early Jurassic (e.g., Trecalli et al., 2012; Li-X et al., 2021). In those instances, widespread crises of shallow water carbonate precipitation at negative carbon-isotope excursions were explained by decreased carbonate saturation of seawater due to ocean acidification, and were followed by the deposition of oolitic limestones. The mechanism proposed to explain this evidence, is that the carbonate precipitation crisis was followed by a rise in the saturation of water with respect to carbonate that promoted chemical precipitation (calcification overshoot of Kump et al., 2009), and therefore the deposition of oolitic bodies. The ooid-rich units characterizing the HST of the CAR 2 depositional sequence in Sichuan and in the Dolomites could therefore be the physical expression of a calcification overshoot following a transient lowering of carbonate saturation, and therefore may indirectly indicate that an ocean acidification phase was associated to, or lasted until, the third CPE NCIE (Fig. 5). This remains a hypothesis that requires further independent confirmation. However, a scenario implying variations in seawater chemistry at the scale of the entire Tethys is consistent with observations by Jin et al. (2020). These authors pointed out that the CPE coincided with a general demise in the precipitation of microbial calcification that was replaced by the production of skeletal carbonates. Microbial precipitation, recovered later, during the Tuvalian after the CPE. Our observations, instead, show that raises and decreases of carbonate production also occurred within the CPE. This evidence, in agreement with the multi-phase nature of the CPE, suggests that multiple fluctuations of carbonate saturation might have occurred during this phase of global climate change.

6. Conclusions

This paper provides detailed facies analysis and new bio-chronostratigraphy based on conodonts, foraminifers and radiometric dating of the Carnian succession of Hanzeng (Sichuan Basin). The bio-chronostratigraphic framework, paired with new stable carbon isotope data and review of several Carnian successions worldwide highlights that during the CPE an eustatic sea-level fall that can be dated to the Julian time. Facies analysis and sequence stratigraphy comparison of the studied succession of the Sichuan Basin, in the eastern Tethys, with the coeval counterpart in the Dolomites of Italy, in the eastern Tethys, reveals a Tethys wide commonality in facies evolution of shallow water carbonate systems during the sea-level rise after the Julian sea level fall. During the CPE a deepening phase (TST of CAR 2 depositional sequence) after the subaerial exposure of carbonate platforms caused by the eustatic fall was followed by a broadly synchronous deposition of thick oolitic bodies (HST of CAR 2 depositional sequence). Such observation testifies that carbonate production experienced a decrease and then a recovery at the Tethys scale that can be bracketed between the onset, and the third negative $\delta^{13}C$ shift of the CPE. The almost synchronous deposition of oolitic bodies in areas located at the extremities of the Tethys Ocean may be evidence of a "precipitation overshoot", analogous to what has been observed in the geologic record following times of ocean acidification. Such evidence suggests that multiple fluctuations of seawater chemistry may have occurred during the Carnian Pluvial Episode.

Acknowledgements

We thank for Stefano Castelli (University of Padova) for realizing the conodont plate, Lu Han and Bin Chen (Chengdu University of Technology), and Qiangwang Wu (University of Padova) helped to collect samples in the NW Sichuan Basin. Prof. Jinyong Xu (Chengdu University of Technology) is thanked for his help with carbon isotope analyses. We are grateful to the editor Prof. Boswell Wing, and two anonymous reviewers for their constructive comments. Special thanks to Prof. David B. Kemp (CUG Wuhan) and Prof. Zhaokun Yan (East China University of Technology) for helpful discussions. This work was supported by National Natural Science Foundation of China (grant numbers 41902106 and 41572085); State Key Laboratory of Marine Geology, Tongji University (grant number MG201903); State Key Laboratory of Loess and Quaternary Geology (grant number SKLLQGZR2005).

Figure captions

Fig. 1. A) The Carnian palaeogeographical map of South China (modified from Ma et al., 2009). The green marker represents the location of the Hanzeng section. WSB: Western Sichuan Basin; DS: deep sea; SS: shallow sea; CSS: coast to shallow sea; GU: gulf; CS: coastal swamp; TF: tidal flat; RS: reef mound and shoal; AP: alluvial plain; AF: alluvial fan; PA: paleoland; CO: coast; UA: uplift area. **B**) Geological map (modified from 1:50000 Geological Map of the Jiangyou Map Sheet published in regional geological survey report, 1996) showing the location of the Hanzeng (green marker) and Huanglianqiao (yellow marker) sections in the Hanzeng area. D: Devonian; C: Carboniferous; P: Permian; J: Jurassic; T_1f: Feixianguan Fm., Lower Triassic; T_1j: Jialinjiang Fm., Lower Triassic; T_2l: Leikoupo Fm.; T_2tj: Tianjingshan

Fm.; T_3m: Ma'antang Fm.; Q: Quaternary. **C**) Lithological column and typical facies of Ladinian- Carnian (Tianjingshan Fm.), Carnian (Ma'antang Fm.) and early Norian (XTZ, Xiaotangzi Fm., modified from Jin et al., 2019). The red wavy line represents the flexural forebulge unconformity follows Jin et al. (2019).

Fig. 2. Microfacies, $\delta^{13}C$, $\delta^{18}O$, and bio-chronostratigraphy of the Hanzeng section. Three negative carbon isotopic excursions (hNCIE1 to 3) are identified. The descriptions of the microfacies (MF) F1 to C3 are shows in the Supplemental Dataset. M = Mudstone; W = Wackestone; P = Packstone; G = Grainstone; F = Floatstone; B = Boundstone; HST = Highstand System Tract; LST = Lowstand System Tract; Mfz = Maximum flooding zone; CPE = Carnian Pluvial Episode; FAD = First Appearance Datumus. In the $\delta^{13}C$ data, black dots refer to samples whose $\delta^{18}O$ values are within the range of articulate brachiopod $\delta^{18}O$ values reported by Korte et al. (2005) and are therefore considered little affected by diagenesis. Gray dots are instead samples that are thought to be altered because of diagenetic phenomena. Blue line is locally weighted scatterplot smoothing (LOWESS) of non-diagenetic $\delta^{13}C$ values above Karst 2. The NCIE 1 and NCIE2 of the CPE are not preserved in this section.

Fig. 3. Record of the Julian eustatic sea-level fall in the marine (Tethyan and Boreal) and continental realms (Pangaea). 1. Dolomites (Dal Corso et al., 2018, and references therein); 2. Julian Alps (Dal Corso et al., 2018, and references therein); 3. Northern Calcareous Alps (Mueller et al., 2016); 4. Sichuan Basin (this work); 5.

Barents Sea (Klausen et al., 2020); 6. Central European Basin (CEB, Zhang et al., 2020); 7. Aghdarband Basin (AB, Northeast Iran, Mazaheri-Johari et al., 2022); 8. Iberia and Balearic Islands (Ortì et al., 2017). G+RS = Göstling Mb. and Reingraben Shales. Paleogeographic location of the succession is shown on map of Carnian (Late Triassic) from Scotese (2014).

Fig. 4. Bio- chemo- and sequence stratigraphic correlation of the Hanzeng section (31°47' N; 104°37' E) in the Sichuan Basin with coeval sections of Torri del Falzarego (46°31'40" N; 12°1'18" E) and Dibona+Milieres (46°32'2" N; 12°4'20" E) in the Western Dolomites. The organic carbon isotope records from the marine successions of the Western Tethys are taken from Dal Corso et al. (2018). Lad. = Ladinian; Ju. = Julian; Tuv. = Tuvalian; Tjs = Tianjingshan Fm.; Trav. = Travenanzes Fm.; Lag. = Lagazuoi Member. Paleogeographic map of Carnian (Late Triassic) is based on Scotese (2014).

Fig. 5. Schematic representation of how carbonate production might have evolved in shallow water marine environments during the transgressive part of the CAR2 sequence. The $\delta^{13}C_{TOC}$ curve is a composite from Dal Corso et al. (2018). The hypothesized calcification overshoot within the CAR 2 sequence precedes the recovery of microbial carbonate production that has been observed after the CPE and that did not happen prior the end of the Tuvalian (Jin et al., 2020). WT = western Tethys; ET = eastern Tethys.

References

Baranyi, V., Miller, C.S., Ruffell, A., Hounslow, M.W., Kürschner, W.M., 2019. A continental record of the Carnian Pluvial Episode (CPE) from the Mercia Mudstone Group (UK): palynology and climatic implications. J. Geol. Soc.. 176, 149-166. http://dx.doi.org/10.1144/jgs2017-150

Benavente, C.A., Mancuso, A.C., Irmis, R.B., Bohacs, K.M., Matheos, S., 2022. Tectonically conditioned record of continental interior paleoclimate during the Carnian Pluvial Episode: The Upper Triassic Los Rastros Formation, Argentina. GSA Bull.. 134(1-2), 60-80. https://doi.org/10.1130/B35847.1

Breda, A., Preto, N., 2011. Anatomy of an Upper Triassic continental to marginal- marine system: the mixed siliciclastic–carbonate Travenanzes Formation (Dolomites, Northern Italy). Sedimentology. 58, 1613-1647. https://doi.org/10.1111/j.1365-3091.2011.01227.x

Chablais, J., Martini, R., Kobayashi, F., Stampfli, G.M., Onoue, T., 2011. Upper Triassic foraminifers from Panthalassan carbonate buildups of southwestern Japan and their paleobiogeographic implications. Micropaleontology. 57, 93–124. https://www.jstor.org/stable/41410975

Dal Corso, J., Bernardi, M., Sun, Y., Song, H., Seyfullah, L.J., Preto, N., Gianilla, P., Ruffell, A., Kustatscher, E., Roghi, G., Merico, A., Hohn, S., Schmidt, A.R., Marzoli, A., Newton, Wignall, P.B., Benton, M.J., 2020. Extinction and dawn of the modern world in the Carnian (Late Triassic). Sci. Adv. 6 (38), eaba0099. https://doi.org/10.1126/sciadv.aba0099

Dal Corso, J., Gianolla, P., Rigo, M., Franceschi, M., Roghi, G., Mietto, P., Manfrin, P., Raucsik, B., Budai, T., Jenkyns, H.C., Reymond, C.E., Caggiati, M., Gattolin, G., Breda, A., Merico, A., Preto, N., 2018. Multiple negative carbon-isotope excursions during the Carnian Pluvial Episode (Late Triassic). Earth. Sci. Rev.. 185, 732-750. https://doi.org/10.1016/j.earscirev.2018.07.004

Furin, S., Preto, N., Rigo, M., Roghi, G., Gianolla, P., Crowley, J. L., Bowring, S.

A., 2006. High-precision U-Pb zircon age from the Triassic of Italy: Implications for the Triassic time scale and the Carnian origin of calcareous nannoplankton and dinosaurs. Geology, 34(12), 1009-1012. https://doi.org/10.1130/G22967A.1

Franceschi, M., Corso, J.D., Cobianchi, M., Roghi, G., Penasa, L., Picotti, V., Preto, N., 2019. Tethyan carbonate platform transformations during the Early Jurassic (Sinemurian–Pliensbachian, Southern Alps): Comparison with the Late Triassic Carnian Pluvial Episode. Geol. Soc. Am. Bull.. 131(7-8), 1255-1275. https://doi.org/10.1130/B31765.1

Gattolin, G., Preto, N., Breda, A., Franceschi, M., Isotton, M., Gianolla, P., 2015. Sequence Stratigraphy after the demise of a high-relief carbonate platform (Carnian of the Dolomites): sea-level and climate disentangled. Palaeogeogr., Palaeoclimatol., Palaeoecol.. 423, 1-17. https://doi.org/10.1016/j.palaeo.2015.01.017

Gianolla, P., De Zanche, V., Mietto, P., 1998. Triassic sequence stratigraphy in the Southern Alps (northern Italy): definition of sequences and basin evolution. In: de Graciansky, P.C., Hardenbol, J., Jacquin, T., Vail, P.R. (Eds.), Mesozoic and Cenozoic Sequence Stratigraphy of European Basins. SEPM Special Publications, 719–747. https://doi.org/10.2110/pec.98.02.0719.

Gianolla, P., De Zanche, V., Roghi, G., 2003. An upper Tuvalian (Triassic) platform–basin system in the Julian Alps: the start-up of the Dolomia Principale (Southern Alps, Italy). Facies. 49, 135-150. http://dx.doi.org/10.1007/s10347-003-0029-7

Hallam, A., Wignall, P. B., 1999. Mass extinctions and sea-level changes. Earth-Sci. Rev.. 48(4), 217-250. https://doi.org/10.1016/S0012-8252(99)00055-0

Haq, B. U., 2018. Triassic eustatic variations reexamined. GSA Today. 28(12), 4-9.

http://dx.doi.org/10.1130/GSATG381A.1

Hornung, T., Brandner, R., Krystyn, L., Joachimski, M. M., Keim, L., 2007. Multistratigraphic constraints on the NW Tethyan "Carnian Crisis". New Mexico Mus. Nat. Hist. Sci. Bull., 4, 9-67.

Jin, X., Gianolla, P., Shi, Z., Franceschi, M., Caggiati, M., Du, Y., Preto, N., 2020. Synchronized changes in shallow water carbonate production during the Carnian Pluvial Episode (Late Triassic) throughout Tethys. Glob. Planet. Change.184, 103035. https://doi.org/10.1016/j.gloplacha.2019.103035

Jin, X., McRoberts, A,C., Shi, Z.Q., Mietto, P., Rigo, M., Roghi, G., Manfrin, S., Franceschi, M., Preto, N., 2019. The aftermath of the CPE and the Carnian/Norian transition in northwestern Sichuan Basin, South China. J. Geol. Soc.. 176, 179-196. https://doi.org/10.1144/jgs2018-104

Klausen, T.G., Paterson, N.W., Benton, M.J., 2020. Geological control on dinosaurs' rise to dominance: Late Triassic ecosystem stress by relative sea level change. Terra Nova. 32(6), 434-441. http://dx.doi.org/10.1111/ter.12480

Korte, C., Kozur, H.W., Veizer, J., 2005. $\delta^{13}C$ and $\delta^{18}O$ values of Triassic brachiopods and carbonate rocks as proxies for coeval seawater and palaeotemperature. Palaeogeogr., Palaeoclimatol., Palaeoecol.. 226, 287–306. http://dx.doi.org/10.1016/j.palaeo.2005.05.018

Kozur, H. W., Bachmann, G. H., 2010. The Middle Carnian Wet Intermezzo of the Stuttgart Formation (Schilfsandstein), Germanic Basin. Palaeogeogr. Palaeoclimatol. Palaeoecol.. 290. 1-4, 107-119. https://doi.org/10.1016/j.palaeo.2009.11.004

Kump, L.R., Bralower, T.J., Ridgwell, A., 2009. Ocean acidification in deep time. Oceanogr.. 22(4), 94-107. http://dx.doi.org/10.5670/oceanog.2009.100

Lein, R., Krystyn, L., Richoz, S., Lieberman, H., 2012. Middle Triassic platform/basin transition along the Alpine passive continental margin facing the Tethys Ocean – The Gamsstein: The rise and fall of a Wetterstein Limestone Platform (Styria, Austria). Journal of Alpine Geology. 54, 471–498.

Li, Y., Yan, Z., Liu, S., Li, H., Cao, J., Su, D., Dong, S.L., Sun, W., Yang, R.J., Yan, L., 2014. Migration of the carbonate ramp and sponge buildup driven by the orogenic wedge advance in the early stage (Carnian) of the Longmen Shan foreland basin, China. Tectonophysics. 619, 179-193. http://dx.doi.org/10.1016/j.tecto.2013.11.011

Li, Q., Ruhl, M., Wang, Y.D., Xie, X.P., An, P.C., Xu, Y.Y., 2021. Response of Carnian Pluvial Episode evidenced by organic carbon isotopic excursions from western Hubei, South China. Palaeoworld. https://doi.org/10.1016/j.palwor.2021.08.004

Li, X., Trower, E. J., Lehrmann, D. J., Minzoni, M., Kelley, B. M., Schaal, E. K., Altiner, D., Yu, M., Payne, J. L., 2021. Implications of giant ooids for the carbonate chemistry of Early Triassic seawater. Geology. 49(2), 156-161. https://doi.org/10.1130/G47655.1

Lu, J., Zhang, P., Dal Corso, J., Yang, M., Wignall, P. B., Greene, S. E., Shao, L., Lyu, D., Hilton, J., 2021. Volcanically driven lacustrine ecosystem changes during the Carnian Pluvial Episode (Late Triassic). Proc. Natl. Acad. Sci.. 118(40). https://doi.org/10.1073/pnas.2109895118

Ma, Y., Chen, H., Wang, G. 2009. Atlas of Tectonics and Sequence Lithofacies Palaeogeography in South China from Sinian to Neogene. Science Press, Beijing, 1–301 [in Chinese].

Mazaheri-Johari, M., Gianolla, P., Mather, T.A. Frieling, J., Chu, D., Dal Corso, J. 2021. Mercury deposition in Western Tethys during the Carnian Pluvial Episode (Late Triassic). Sci. Rep.. 11, 17339. https://doi.org/10.1038/s41598-021-96890-8

Mazaheri-Johari, M., Roghi, G., Caggiati, M., Kustatscher, E., Ghasemi-Nejad, E., Zanchi, A., Gianolla, P., 2022. Disentangling climate signal from tectonic forcing: The Triassic Aghdarband Basin (Turan Domain, Iran). Palaeogeogr., Palaeoclimatol., Palaeoecol.. 586, 110777. https://doi.org/10.1016/j.palaeo.2021.110777

Metcalfe, I., 2013. Gondwana dispersion and Asian accretion: Tectonic and palaeogeographic evolution of eastern Tethys. J. Asian Earth Sci.. 66, 1-33. https://doi.org/10.1016/j.jseaes.2012.12.020

Mueller, S., Krystyn, L., Kürschner, W.M., 2016. Climate variability during the Carnian Pluvial Phase - A quantitative palynological study of the Carnian sedimentary succession at Lunz am See, Northern Calcareous Alps, Austria. Palaeogeogr., Palaeoclimatol., Palaeoecol.. 441, 198–211. http://dx.doi.org/10.1016/j.palaeo.2015.06.008

Ortí, F., Pérez-López, A., Salvany, J. M., 2017. Triassic evaporites of Iberia: Sedimentological and palaeogeographical implications for the western Neotethys evolution during the Middle Triassic–Earliest Jurassic. Palaeogeogr., Palaeoclimatol., Palaeoecol.. 471, 157-180. https://doi.org/10.1016/j.palaeo.2017.01.025

Preto, N., Hinnov, L.A., 2003. Unraveling the origin of carbonate platform cyclothems in the Upper Triassic Durrenstein Formation (Dolomites, Italy). J. Sediment. Res.. 73, 774-789. http://dx.doi.org/10.1306/030503730774

Rettori, R., Loriga, C., Neri, C., 1998. Lower Carnian foraminifers from the type locality of the Calcare del Predil (Raibl group, northeastern Italy). Riv. Ital. Paleontol. Stratigr., 104(3), 369-380. https://doi.org/10.13130/2039-4942/5341

Rigaud, S., Martini, R, Rettori, R., 2012. Parvalamellinae, a new subfamily for Triassic glomospiroid Involutinidae. J. Foramin. Res.. 42(3), 245-256. https://doi.org/10.2113/gsjfr.42.3.245

Rigo, M., Preto, N., Franceschi, M., Guaiumi, C., 2012. Stratigraphy of the Carnian-Norian Calcari con Selce Formation in the Lagonegro Basin, Southern Apennines. Riv. Ital. Paleontol. Stratigr.. 118, 143- 154. https://doi.org/10.13130/2039-4942/5995

Rigo, M., Mazza, M., Karádi, V., Nicora, A., 2018. New Upper Triassic Conodont Biozonation of the Tethyan Realm. In L.H. Tanner (Ed.), The Late Triassic World: Earth in a Time of Transition. Springer, Berlin, pp. 189-235.

Rigo, M., Preto, N., Roghi, G., Tateo, F., Mietto, P., 2007. A rise in the Carbonate Compensation Depth of western Tethys in the Carnian (Late Triassic): Deep-water evidence for the Carnian Pluvial Event. Palaeogeogr., Palaeoclimatol., Palaeoecol.. 246, 188-205. https://doi.org/10.1016/j.palaeo.2006.09.013

Rubatto, D., Gebauer, D., 2000. Use of cathodoluminescence for U–Pb zircon dating by ion microprobe: some examples from the Western Alps. In: Pagel, M., Barbin, V., Blanc, P., Ohnenstetter, D. (Eds.), Cathodoluminescence in Geosciences. Springer, Berlin, pp. 373-400.

Schmitz, M.D., Davydov, V.I., 2012. Quantitative radiometric and biostratigraphic calibration of the Pennsylvanian–Early Permian (Cisuralian) time scale and pan-Euramerican chronostratigraphic correlation. Geol. Soc. Am. Bull.. 124(3-4), 549-577. https://doi.org/10.1130/B30385.1

Scotese, C. R., 2014. Atlas of Middle & Late Permian and Triassic Paleogeographic Maps, maps 43 - 48 from Volume 3 of the PALEOMAP Atlas for ArcGIS (Jurassic and Triassic) and maps 49 – 52 from Volume 4 of the PALEOMAP PaleoAtlas for ArcGIS (Late Paleozoic), Mollweide Projection, PALEOMAP Project, Evanston, IL.

Shi, Z.Q., Jin. X., Preto. N., Rigo, M., Du, Y.X., Han, L., 2019. The Carnian Pluvial Episode at Ma'antang, Jiangyou in Upper Yangtze Block, Southwestern China. J. Geol. Soc.. 176, 197-207. https://doi.org/10.1144/jgs2018-038

Simms, M.J., Ruffell, A.H., 1989. Synchroneity of climatic change and extinctions in the Late Triassic. Geology. 17, 265. https://doi.org/10.1130/0091-7613(1989)017<0265:SOCCAE>2.3.CO;2

Stefani, M., Furin, S., Gianolla, P., 2010. The changing climate framework and depositional dynamics of Triassic carbonate platforms from the Dolomites. Palaeogeogr., Palaeoclimatol., Palaeoecol.. 290, 43-57. https://doi.org/10.1016/j.palaeo.2010.02.018

Sun, Y.D., Wignall, P.B., Joachimski, M.M., Bond, D.P.G., Grasby, S.E., Lai, X.L., Wang, L.N., Zhang, Z.T., Sun, S., 2016. Climate warming, euxinia and carbon isotope perturbations during the Carnian (Triassic) Crisis in South China. Earth

Planet. Sci. Lett.. 444, 88-100. https://doi.org/10.1016/j.epsl.2016.03.037

Tomimatsu, Y., Nozaki, T., Sato, H., Takaya, Y., Kimura, J. I., Chang, Q., Naraoka, H., Rigo, M., Onoue, T., 2021. Marine osmium isotope record during the Carnian “pluvial episode” (Late Triassic) in the pelagic Panthalassa Ocean. Glob. Planet. Change. 197, 103387. https://doi.org/10.1016/j.gloplacha.2020.103387

Trotter, J. A., Williams, I. S., Nicora, A., Mazza, M., Rigo, M., 2015. Long-term cycles of Triassic climate change: a new $\delta^{18}O$ record from conodont apatite. Earth. Planet. Sci. Lett.. 415, 165–174. https://doi.org/10.1016/j.epsl.2015.01.038

Vigran, J.O., Mangerud, G., Mørk, A., Worsley, D., Hochuli, P.A., 2014. Palynology and geology of the Triassic succession of Svalbard and the Barents Sea. Geol. Surv. Norway Spec. Publ. 14, 1–247

Wu, X., 1989. Carnian (Upper triassic) sponge mounds of the Northwestern Sichuan Basin, China: Stratigraphy, facies and paleoecology. Facies. 21, 171-187. https://doi.org/10.1007/BF02536835

Yan, Z.K., Tian, Y.T., Li, R., Vermeesch, P., Sun, X.L., Li, Y., Rittner, M., Carter, A., Shao, C.J., Huang, H., Ji, X.T., 2019. Late Triassic tectonic inversion in the upper Yangtze Block: insights from detrital zircon U–Pb geochronology from South-Western Sichuan Basin. Basin Res.. 31, 92–113. https://doi.org/10.1111/bre.12310

Zhang, Y., Ogg, J. G., Franz, M., Bachmann, G. H., Szurlies, M., Röhling, H. G., Li, M., Rolf, C., Obst, K., 2020. Carnian (Late Triassic) magnetostratigraphy from the Germanic Basin allowing global correlation of the Mid-Carnian Episode. Earth Planet. Sci. Lett.. 541, 116275. https://doi.org/10.1016/j.epsl.2020.116275

Figure 1

Click here to access/download;Figure;Fig. 1.pdf

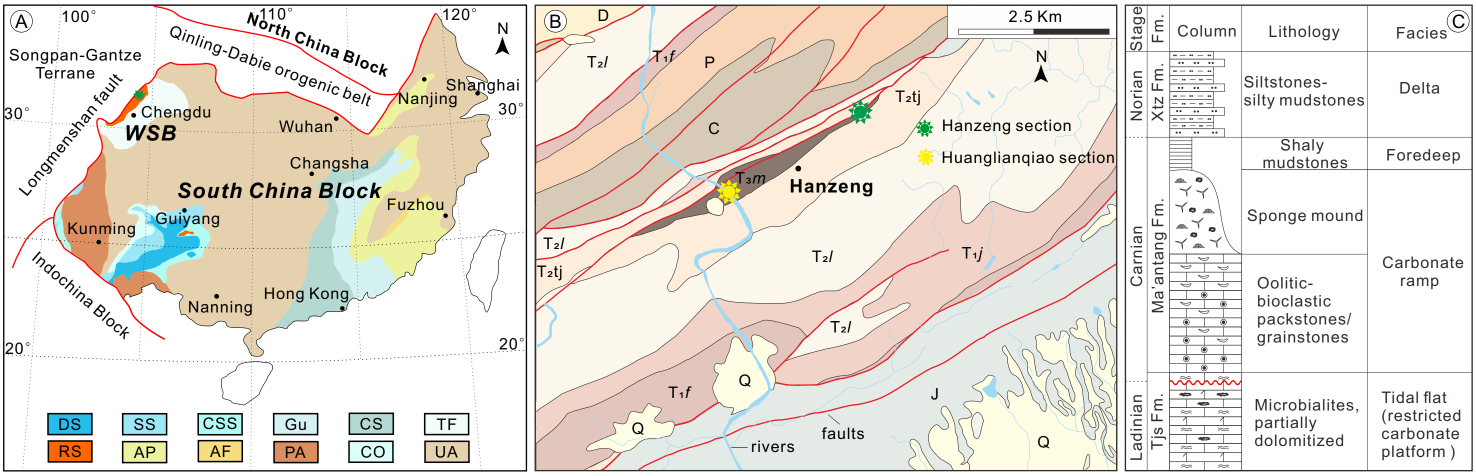

Figure 2

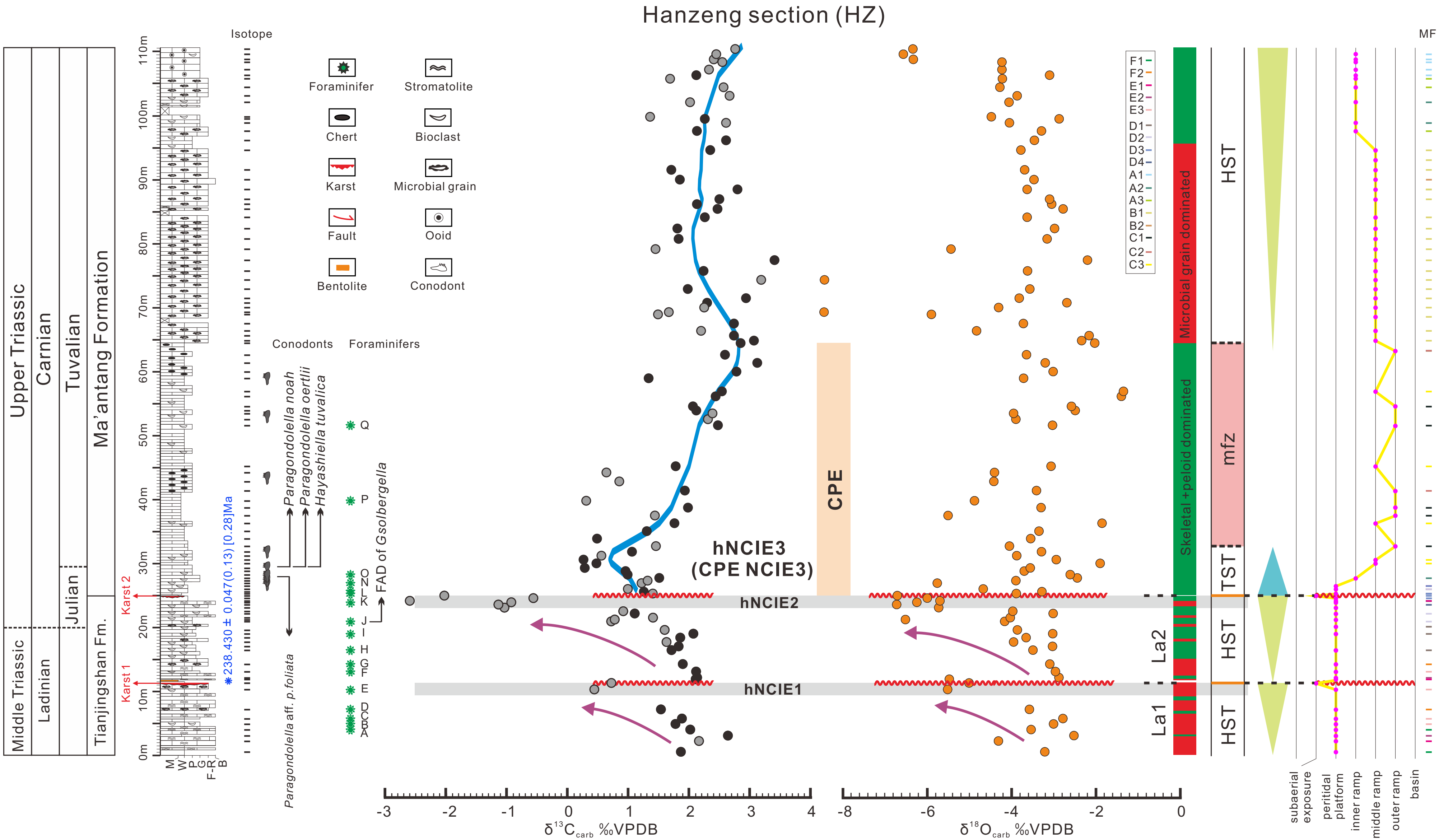

Hanzeng section (HZ)
Upper Triassic
Middle Triassic
Carnian
Ladinian
Tuvalian
Julian
Ma'antang Formation
Tianjingshan Fm.
Isotope
Conodonts
Foraminifers
Foraminifer
Stromatolite
Chert
Bioclast
Karst
Microbial grain
Fault
Ooid
Bentolite
Conodont
Karst 2
Karst 1
238.430 ± 0.047(0.13) [0.28]Ma
Paragondolella noah
Paragondolella oertlii
Hayashiella tuvalica
Paragondolella aff. p.foliata
FAD of Gsolbergella
hNCIE3
(CPE NCIE3)
hNCIE2
hNCIE1
CPE
δ13Ccarb ‰VPDB
δ18Ocarb ‰VPDB
Microbial grain dominated
Skeletal+peloid dominated
HST
mfz
TST
La2
La1
MF
subaerial exposure
peritidal platform
inner ramp
middle ramp
outer ramp
basin

Figure 3

Click here to access/download;Figure;Fig. 3.pdf

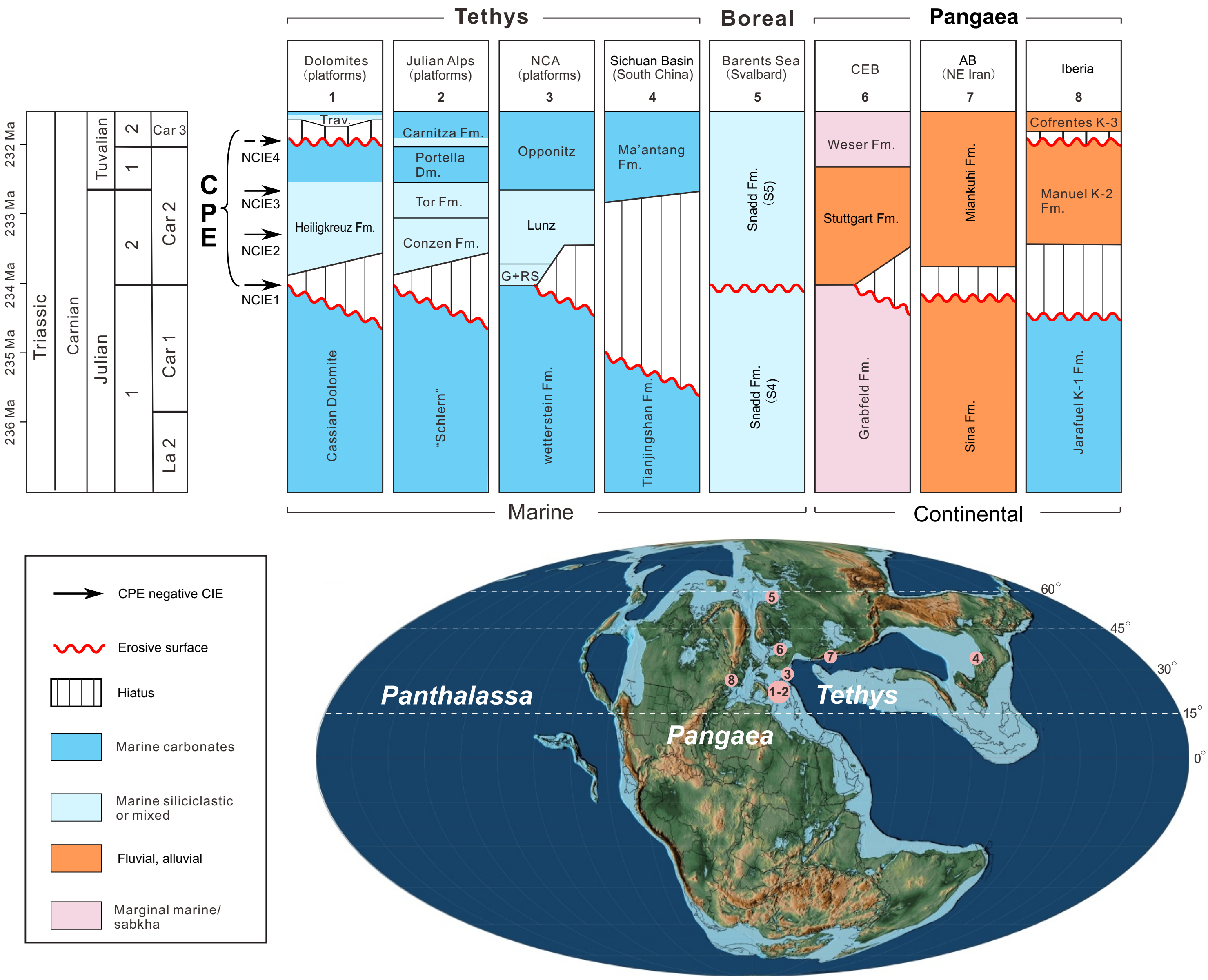

Figure 4

Click here to access/download;Figure;Fig. 4.pdf

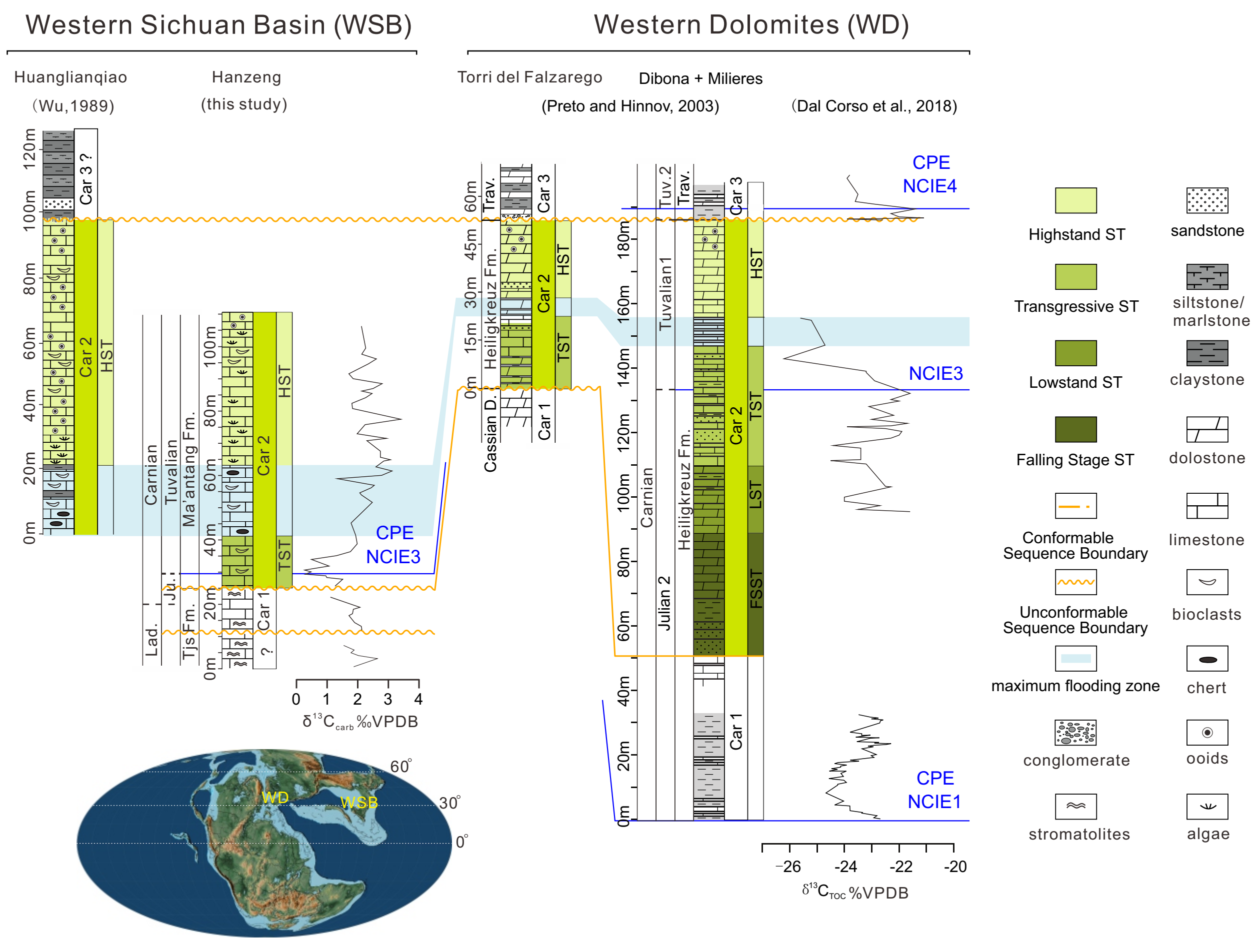

Figure 5

Click here to access/download;Figure;Fig. 5.pdf

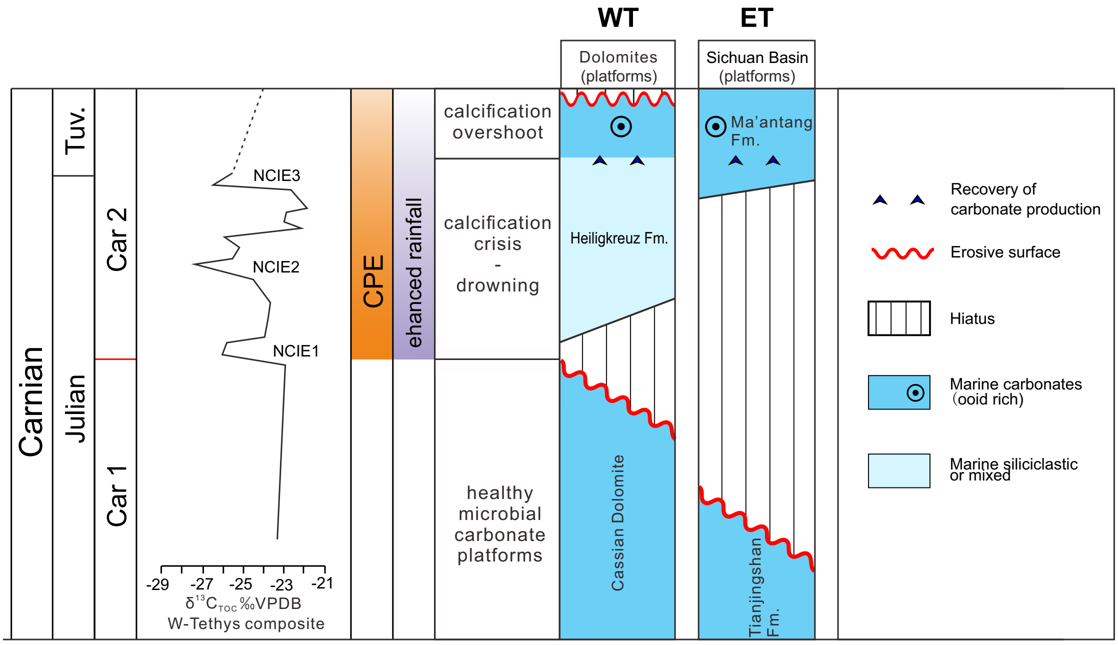

Figure S1

Click here to access/download
Supplementary material for online publication only
Fig.S1.pdf

Figure S2

Click here to access/download
Supplementary material for online publication only
Fig.S2.pdf

Figure S3

Figure S4

Figure S5

Click here to access/download
Supplementary material for online publication only
Fig.S5.pdf

Figure S6

Figure S7

Click here to access/download

Supplementary material for online publication only

Fig.S7.pdf

Figure SI1

Figure SI2

Data

Click here to access/download
Raw research data (under CC BY license see above)
Supplemental Dataset.xlsx

Declaration of interests

☐ The authors declare that they have no known competing financial interests or personal relationships that could have appeared to influence the work reported in this paper.

☐The authors declare the following financial interests/personal relationships which may be considered as potential competing interests:

The authors declare that they have no known competing financial interests or personal relationships that could have appeared to influence the work reported in this paper.

Credit Author Statement of the paper

Eustatic sea-level fall and global fluctuations in carbonate production during the Carnian Pluvial Episode by Xin Jin et al.

This study involved collaboration among several experts as reflected in the authorship of the submitted paper. Here are their roles:

Xin Jin - participated in all field works, and collected and prepared conodonts, measured all the carbon-isotopic samples and LA-ICP-MS U-Pb zircon sample, draw the graphics, wrote the text.

Marco Franceschi - participated in field works, draw the graphics, wrote the text.

Rossana Martini – classified foraminifers and wrote the relevant part, reviewed and modified the text.

Zhiqiang Shi - participated in field works, reviewed and modified the text.

Piero Gianolla – provided sequence stratigraphic interpretation, reviewed and modified the text.

Manuel Rigo - classified conodonts and wrote the relevant part, reviewed and modified the text.

Corey J. Wall - measured the CA-ID-TIMS U-Pb zircon sample, wrote, reviewed and modified the analytical method of the CA-ID-TIMS.

Mark D. Schmitz - measured the CA-ID-TIMS U-Pb zircon sample, wrote, reviewed and modified the analytical method of the CA-ID-TIMS.

Gang Lu - processed original U-Pb zircon data, reviewed and modified the text.

Yixing Du - classified conodonts and wrote the relevant part, reviewed and modified the text.

Xiangtong Huang- measured the LA-ICP-MS U-Pb zircon sample, wrote, reviewed and modified the analytical method of the LA-ICP-MS.

Nereo Preto - participated in field works, described microfacies, designed this study, wrote, reviewed and modified the text.